the
abdus salam
international
centre
for theoretical
physics

united nations
educational, scientific
and cultural
organization

international atomic
energy agency

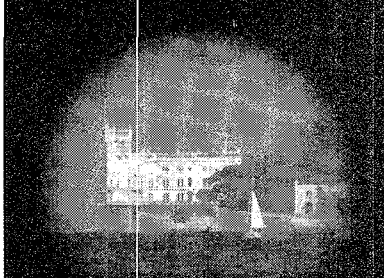

preprint

ELECTRONIC PROPERTIES OF SINGLE-WALLED CHIRAL CARBON NANOTUBE

S.Y. Mensah

F.K.A. Allotey

N.G. Mensah

and

G. Nkrumah

Available at: http://www.ictp.trieste.it/~pub_off IC/2001/118

United Nations Educational Scientific and Cultural Organization
and
International Atomic Energy Agency
THE ABDUS SALAM INTERNATIONAL CENTRE FOR THEORETICAL PHYSICS

ELECTRONIC PROPERTIES OF SINGLE-WALLED CHIRAL CARBON NANOTUBE

S.Y. Mensah
Department of Physics, Laser and Fibre Optics Centre, University of Cape Coast, Ghana,

F.K.A. Allotey
National Centre for Mathematical Sciences, Ghana Atomic Energy Commission, Kwabenya, Accra, Ghana
and
The Abdus Salam International Centre for Theoretical Physics, Trieste, Italy

N.G. Mensah[1]
Department of Mathematics, University of Cape Coast, Ghana
and
The Abdus Salam International Centre for Theoretical Physics, Trieste, Italy

and

G. Nkrumah
Department of Physics, University of Ghana, Legon, Accra, Ghana.

MIRAMARE – TRIESTE
September 2001

[1]Regular Associate of the Abdus Salam ICTP.

Abstract

The electronic properties of single-walled chiral carbon nanotube has been studied using the model based on infinitely long carbon atoms wrapped along a base helix of single-walled carbon nanotubes(SWNTs). The problem is solved semiclassically, and current density j, resistivity ρ, thermopower α_z and electrical power factor P calculated. It is noted that the current density j displays negative differential conductivity, whiles the resistivity ρ increases with increasing electrical field. ρ also slowly inceases at low temperatures and then gradually increases with increasing temperature. The thermopower α_z shows interesting behaviour. Very intriguing is the electrical power factor which shows relatively large values.

1 Introduction

Carbon nanotubes (CNTs) are newly discovered materials, which have unique electrical and mechanical properties[1]. Carbon nanotubes are fullerenes with carbon atoms situated regularly on helical lattice sites[2]. The base helix of the helical lattice is wrapped along the surface of a cylinder of cross-sectional radius of approximately 10–150 Å. The wrapping angle, also called the geometric chiral angle (GCA), is usually a few degrees[3]. Exhibiting helical symetry, CNTs are quasi-one-dimensional chiral systems[4, 5]. Reviews and books of fullerenes can be found in [6]−[9].

Electronic properties of CNTs, especially the electron transport[10−14], have received a lot of attention. It is noted that these properties of CNTs are quite different from those of well known carbonic structures such as a planar monoatomic graphite sheet (graphene). They show negative differential conductivity similar to that of superlattice. They also display metallic conductivity. In fact, this behaviour can be attributed to its dependence on the cross-sectional radius and the geometrical chiral angle. In [15, 4], temperature dependent dc and ac eletrical restivity ρ of macroscopic mats and single-walled carbon nanotubes (SWNTs) were measured. They showed qualitatively similar behaviour: at high temperatures, they are metallic and exhibit a cross over to nonmetallic at low temperatures. The cross over temperature varied from sample to sample and sensitive to mechanical handling. Similar measurement were made in [16]. Furthermore, in [17]−[19] electronic and electromagnetic properties of nanotubes were studied extensively. In [19] the dependence of the current chiral angle (CCA) on the ac eletric field amplitude was elucidated for the electron transport. They noted that at certain amplitudes of the ac electric field, the axial component of the time-varying current vanished and the circumferential component remained.

Another interesting transport property that is worth studying and currently receiving a lot of attention is the thermoelectrical properties. In [20] L. Grigorian et al have observed experimentally giant thermopower in carbon nanotubes.They assigned the contribution from the large thermopower peak to the presence of magnetic impurities within the bundles. This general phenomenom is known as the "Kondo effect". Sumanasekera et al [21] have reported on the effect of gas adsorption and collisions on the thermopower and resistivity of mats of tangled SWNT. Their results indicated that previously published large positive thermopower data should not be assigned to intrinsic SWNT behaviour but to transport in oxygen-doped SWNTs. Further theoretical study by Mensah et al [22] on the differential thermopower of a chiral carbon nanotube showed that the thermopower α of the CNT can be semimetallic, p-type semiconductor or n-type semiconductor depending on the parameters of the CNT and therefore proposed the use of CNT as thermoelement.

In this paper, we further probe the results obtained in [22] by analysing the current density j, resistivity ρ and the power factor P, and thus confirming our proposed use of CNT as a thermoelement.

This paper is organised as follows: in section 2 we establish the theory and solution of the problem and in section 3 we discuss the results and draw conclusions.

2 Theory

We proceed as in [17, 19] by considering an infinitely long chain of carbon atoms wrapped along a base helix as a model of a SWNT. The chief merit of this model is its analytical tractability, which readily yields physically interpretable results. Secondly, the model yields correct qualitative description of various electronic processes which are corroborated by first principle numerical simulations.

The problem is considered in the semiclassical approach by commencing with the Boltzmann kinetic equation [23],

$$\frac{\partial f(r,p,t)}{\partial t} + v(p)\frac{\partial f(r,p,t)}{\partial r} + eE\frac{\partial f(r,p,t)}{\partial p} = -\frac{f(r,p,t) - f_o(p)}{\tau}. \tag{1}$$

Here $f(r,p,t)$ is the distribution function; $f_o(p)$ is the equilibrium distribution function; $v(p)$ is the electron velocity; E is the constant applied electric field; r is the electron position, p is the electron dynamical momentum; τ is the electron relaxation time and e is the electron charge.

The collision integral is taken in the τ approximation and further assumed constant. The exact solution of Eq.(1) presents some difficulties. We therefore solved it using perturbation approach with the second term treated as the perturbation. In the linear approximation of ∇T and $\nabla\mu$, we obtain

$$\begin{aligned} f(p) &= \tau^{-1}\int_0^\infty \exp\left(-\frac{t}{\tau}\right) f_o(p - eEt)dt + \int_0^\infty \exp\left(-\frac{t}{\tau}\right) dt \\ &\cdot \left([\varepsilon(p - eEt) - \mu]\frac{\nabla T}{T} + \nabla\mu\right) v(p - eEt)\frac{\partial f_o(p-eEt)}{\partial\varepsilon}, \end{aligned} \tag{2}$$

$\varepsilon(p)$ is the energy of the electron, and μ is the chemical potential. Seeking the current density in the form

$$\mathbf{j} = e\sum_p \mathbf{v}(p)f(p), \tag{3}$$

we make the transformation

$$p - eEt \to p,$$

and then resolve the currnt along the tubular axis (z-axis) and the base helix respectively, neglecting the interference between the axial and the helical paths connecting a pair of atoms, and thus ignoring transverse motion quantization. Using the following transformation,

$$\sum_p \to \frac{2}{(2\pi\hbar)^2}\int\int dp_s dp_z,$$

the electron current density along the tubular axis and the base helix are obtained as

$$Z' = \frac{2e^2\tau^{-1}}{(2\pi\hbar)^2}\int_0^\infty \exp\left(-\frac{t}{\tau}\right) dt \int\int v_z\left(p_z - eE_z t\right) f_o(p) dp_s dp_z$$

$$+\frac{2e^2}{(2\pi\hbar)^2}\int_0^\infty \exp\left(-\frac{t}{\tau}\right)dt\int\int\left([\varepsilon(p)-\mu]\frac{\nabla_z T}{T}+\nabla_z\mu\right)$$
$$\cdot\left(v_z\left(p_z\right)\frac{\partial f_o(p)}{\partial\varepsilon}\right)v_z\left(p_z-eE_z t\right)dp_s dp_z \tag{4}$$

and

$$S' = \frac{2e^2\tau^{-1}}{(2\pi\hbar)^2}\int_0^\infty \exp\left(-\frac{t}{\tau}\right)dt\int\int v_s\left(p_s-eE_s t\right)f_o(p)dp_s dp_z$$
$$+\frac{2e^2}{(2\pi\hbar)^2}\int_0^\infty \exp\left(-\frac{t}{\tau}\right)dt\int\int\left([\varepsilon(p)-\mu]\frac{\nabla_s T}{T}+\nabla_s\mu\right)$$
$$\cdot\left(v_s\left(p_s\right)\frac{\partial f_o(p)}{\partial\varepsilon}\right)v_s\left(p_s-eE_s t\right)dp_s dp_z \tag{5}$$

where the integrations are carried out over the first Brillouin zone. From these two components, expressions for the axial and circumferential components of the current density emerge as follows:

$$j_z = Z' + S'\sin\theta_h, \qquad j_c = S'\cos\theta_h, \tag{6}$$

where, $\theta_\hbar$ is the GCA.

The energy of the electrons, as expressed in [19], is given as

$$\varepsilon(p) = \varepsilon_o - \Delta_z\cos\frac{p_z d_z}{\hbar} - \Delta_s\cos\frac{p_s d_s}{\hbar}, \tag{7}$$

where ε_o is the energy of an outer-shell electron in an isolated carbon atom, Δ_z and Δ_s are the real overlapping integrals for jumps along the respective co-ordinates, p_z and p_s are the carrier momentum along the tubular axis and the base helix respectively, $\hbar$ is the Planck's constant, d_z is the distance between the site n and the site $n+N$ along the tubular axis, and d_s is the distance between the site n and $n+1$ along the base helix.

To calculate the current density for non-degenerate electron gas, we use the Boltzmann equilibrium distribution function expressed as

$$f_o(p) = C\exp-\left(\frac{\varepsilon(p)-\mu}{kT}\right), \tag{8}$$

where

$$C = \frac{d_z d_s \mathrm{n}_o}{2\exp\left(\frac{\mu-\varepsilon_o}{kT}\right)I_0\left(\frac{\Delta_s}{kT}\right)I_0\left(\frac{\Delta_z}{kT}\right)},$$

n_o, is the surface charge density; $I_n(x)$ is the modified Bessel function of order n, and k is the Boltzmann's constant.

The components v_z and v_s of the electron velocity $\mathbf{v}$ are calculated from Eq.(7) as

$$v_z(p_z) = \frac{\partial\varepsilon}{\partial p_z} = \frac{\Delta_z d_z}{\hbar}\sin\left(\frac{p_z d_z}{\hbar}\right), \tag{9}$$

and

$$v_s(p_s) = \frac{\partial\varepsilon}{\partial p_s} = \frac{\Delta_s d_s}{\hbar}\sin\left(\frac{p_s d_s}{\hbar}\right) \tag{10}$$

With the help of Eq.(4)-Eq.(10) and the fact that $E_s = E_z \sin\theta_h$ and $\nabla_s T = \nabla_z T \sin\theta_h$, we obtain for the axial j_z and circumferential j_c currents after cumbersome calculation, the following expression

$$\begin{aligned} j_z &= \left(\sigma_z(E) + \sigma_s(E)\sin^2\theta_h\right)\nabla_z\left(\frac{\mu}{e} - \phi\right) \\ &- \left\{\sigma_z(E)\frac{k}{e}\left(\frac{\varepsilon_o - \mu}{kT} - \Delta_z^*\frac{I_0(\Delta_z^*)}{I_1(\Delta_z^*)} + 2 - \Delta_s^*\frac{I_1(\Delta_s^*)}{I_0(\Delta_s^*)}\right)\right. \\ &\left. + \sigma_s(E)\frac{k}{e}\sin^2\theta_h\left(\frac{\varepsilon_o - \mu}{kT} - \Delta_s^*\frac{I_0(\Delta_s^*)}{I_1(\Delta_s^*)} + 2 - \Delta_z^*\frac{I_1(\Delta_z^*)}{I_0(\Delta_z^*)}\right)\right\}\nabla_z T \end{aligned} \tag{11}$$

$$\begin{aligned} j_c &= \left(\sigma_s(E)\sin\theta_h\cos\theta_h\right)\nabla_z\left(\frac{\mu}{e} - \phi\right) - \sigma_s(E)\frac{k}{e}\sin\theta_h\cos\theta_h \\ &\cdot\left(\frac{\varepsilon_o - \mu}{kT} - \Delta_s^*\frac{I_0(\Delta_s^*)}{I_1(\Delta_s^*)} + 2 - \Delta_z^*\frac{I_1(\Delta_z^*)}{I_0(\Delta_z^*)}\right)\nabla_z T, \end{aligned} \tag{12}$$

where ϕ is the electrostatic potential. From Eqs.(11) and (12) the electrical conductivities are given as

$$\sigma_{zz} = \sigma_z(E) + \sigma_s(E)\sin^2\theta_h \tag{13}$$

$$\sigma_{cz} = \sigma_s(E)\sin\theta_h\cos\theta_h \tag{14}$$

where

$$\begin{aligned} \sigma_z(E) &= \frac{\mathrm{n}_o e^2 \Delta_z d_z^2 \tau I_1(\Delta_z^*)}{\hbar^2\left(1 + (\Omega_z\tau)^2\right) I_0(\Delta_z^*)}; \\ \sigma_s(E) &= \frac{\mathrm{n}_o e^2 \Delta_s d_s^2 \tau I_1(\Delta_s^*)}{\hbar^2\left(1 + (\Omega_s\tau)^2\right) I_0(\Delta_s^*)}; \\ \Omega_z &= \frac{eE_z d_z}{\hbar}; \\ \Omega_s &= \frac{eE_s d_s}{\hbar}; \\ \Delta_i^* &= \frac{\Delta_i}{kT}, \quad i = z,\ s. \end{aligned}$$

The differential thermoelectric power α is defined as the ratio $\frac{|\nabla(\frac{\mu}{e} - \phi)|}{|\nabla T|}$ in an open circuit. Hence interesting to us, α along the axial and circumferential directions are obtained from Eq.(11) and Eq.(12) as

$$\begin{aligned} \alpha_{zz} &= \left[\frac{\sigma_z(E)}{\sigma_z(E) + \sigma_s(E)\sin^2\theta_h}\frac{k}{e}\left\{\frac{\varepsilon_o - \mu}{kT} - \Delta_z^*\frac{I_0(\Delta_z^*)}{I_1(\Delta_z^*)} + 2 - \Delta_s^*\frac{I_1(\Delta_s^*)}{I_0(\Delta_s^*)}\right\}\right. \\ &\left. + \frac{\sigma_s(E)\sin^2\theta_h}{\sigma_z(E) + \sigma_s(E)\sin^2\theta_h}\frac{k}{e}\left\{\frac{\varepsilon_o - \mu}{kT} - \Delta_s^*\frac{I_0(\Delta_s^*)}{I_1(\Delta_s^*)} + 2 - \Delta_z^*\frac{I_1(\Delta_z^*)}{I_0(\Delta_z^*)}\right\}\right] \end{aligned} \tag{15}$$

$$\alpha_{cz} = \frac{k}{e}\left[\frac{\varepsilon_o - \mu}{kT} - \Delta_s^*\frac{I_0(\Delta_s^*)}{I_1(\Delta_s^*)} + 2 - \Delta_z^*\frac{I_1(\Delta_z^*)}{I_0(\Delta_z^*)}\right] \tag{16}$$

3 Discussion and Conclusion

In this paper we studied the electronic properties of SWCNTs, namely the current j, resistivity ρ, thermopower α and electrical power factor P. We do so by solving the Boltzmann's equation and obtaining analytical expressions for the above mentioned properties. As interesting as these properties may be, it is necessary to elucidate their behaviour by presenting them graphically.

Figure 1(a) shows the normalized current density j/j_o with $E^* = ed\tau E/\hbar$ for different values of GCA θ_h. The current rises to maximum and then falls off. Such behaviour is what is described as negative differential conductivity. We noted that the bigger the GCA, the higher the peak value. Figure 1(b) shows the three-dimensional plot of j/j_o as a function of E^* and θ_h.

In figure 2(a) we plotted the resistivity ρ against temperature T. We observed that ρ changes slowly at low temperatures up to 200K and then gradually increases as the temperature rises. Comparing our results with resistivity of rare-earth compounds which are more favoured for themoelements, we noted that our results are low[24]. A three-dimensional plot of ρ against T and $\Omega\tau$ is also presented in figure 2(c).

For the thermpower α_z, we noted that it is highly anisotropic depending on the GCA θ_h, the electric field E, temperature T and the overlapping integrals for the jumps along the respective coordinates Δ_z and Δ_s. Figure 3(a) shows the plot of α_z against T for varying values of Δ_s(measured in eV). Δ_s is varied from 0.015eV to 0.020eV for fixed $\Delta_z = 0.024$eV. When $\Delta_s = 0.015$eV, the curve showed a hyperbolic behaviour. This is expected for semiconducting tubes which exhibit the behaviour $\alpha \sim 1/T$[21]. As Δ_s is increased we noted a peak, and then the curve falls off. The peak drops with increasing values of Δ_s. Interestingly, the peaks occur around 150K to100K and shift towards low temperatures. This behaviour is characteristic of semimetallic materials. The curves in figure 3(b) behave like those of figure 3(a) except that when Δ_z was increased to 0.027eV all the curves behaved like semimetals. In figures 3(c) and 3(d), we show three-demensional plots of α_z against T and Δ_z; and α_z against T and $\Omega\tau$. From the plots it is obvious that α_z decreases strongly with increasing $\Omega\tau$ (i.e. the electric field). For further information about the thermopower α_z see [22].

Lastly but not the least, we studied the power factor which is defined as

$$P = \frac{\alpha^2}{\rho}.$$

This parameter is paramount in the study of thermodevices, be they generators, thermocouples or refrigerators, since the thermoelectric figure of merit Z, is defined by the relation,

$$Z = \frac{P}{\chi},$$

where χ is the thermal conductivity. χ is characterized by electron thermal conductivity and lattice conductivity, the latter playing more important role in the thermal conducativity. In most materials, χ does not lend itself to change, hence they remain fixed. For this reason P becomes the determining factor for the enhancement of Z.

Figure 4(a) shows the plot of P against T for values of $\Omega\tau$ equals 1, 2 and 3. The plot indicates that P has highest peak value for low electric fields, and the peak drops off fast as we increase the electric fields. Similar peaks were observed in figure 4(b) for P against T for different values of Δ_s, i.e. Δ_s ranging from 0.015eV to 0.020eV for a fixed $\Delta_z = 0.027$eV. The highest peak occurs at $\Delta_s = 0.015$eV and falls off as Δ_s increases. The P values are quite big and are measured in W/mK^2 as against measurement in other materials which are measured in $\mu W/mK^2$. The peaks also occur around150K to100K. Compared with$YbAl_3$ material[25], P is found to be about 5 times bigger when we take the peak value to be $0.04W/mK^2$. In figures 4(c) and 4(d), we present three-dimensional plots of P against T and Δ_z for $\Delta_s = 0.018$eV, and P against T and $\Omega\tau$. P strongly decreases with increase in electric field, implying that optimal value of P is obtained in low field regime.

In conclusion, we have studied the electronic properties of single-walled chiral CNTs and noted that the current-voltage characteristics show a negative differential conductivity. The material has a low resistivity and very interesting thermoelectric properties. The electrical power factor P is quite big and hence we propose the use of the material as a thermoelement.

Acknowledgements

This work was done within the framework of the Associateship Scheme of the Abdus Salam International Centre for Theoretical Physics, Trieste Italy. Financial support from the Swedish International Development Cooperation Agency is acknowledged.

References

[1] Iijima S. and Ichihashi, 1993 *Nature* (London) 363 603

[2] Dresselhaus M.S., 1992 *Nature* (London) 358 195

[3] Rodrigue N.M. 1993 *J. Mater. Res.* **8**, 3233

[4] Lin-Chunng P.J and Rajagopal A.K. 1994 *J. Phys. Condens. Matter* **6**, 3697

[5] Lin-Chunng P.J and Rajagopal A.K. 1994 *J. Phys. Rev.* B **49**, 8454

[6] Eletskii A.V. and Smirnov B.M 1993 *Phys. Usp.* **36** (3) 202

[7] Dresselhaus M.S., Dresselhaus G. and Eklund P.C. 1996 *Science of Fullerenes and Carbon Nanotubes* (Academic, New York)

[8] Harris P.J.S 1999 *Carbon Nanotubes and Related Structures, New Materials for the Twenty-first Century* (Cambridge University Press)

[9] Ebbeson T.W. 1997 *Carbon Nanotubes Preparation and Properties* (CRC Press Inc.)

[10] Saito R, Fujita M., Dresselhaus G. and Dresselhaus M.S. 1992 *Phys. Rev,* B **46** 1804

[11] Romanov D.A. and Kibis O.V. 1993 *Phys. Lett.* A **178** 335

[12] Lin MF and Shung K.W.K. 1995 *Phys. Rev.* B **52** 8423

[13] Miyamoto Y., Louie S.G. and Cohen M.L. 1996 *Phys. Rev. Lett.* **76** 2121

[14] Bogachek E.N., Jonson M., Shekhter R.I. and Swahn T. 1993 *Phys. Rev.* B **47** 16635

[15] Fischer J.E. et al 1997 *Phys. Rev.* B **55** R4921

[16] Hone J. et al 1998 *Phys. Rev. Lett.* **80** 1042

[17] Yevtushenko O.M., Slepyan G. Ya, Maksmenko S.A., Lakhtakia A. and Romanov D.A. 1997 *Phys. Rev. Lett.* **79**, 1102

[18] Slepyan G. Ya, Maksimenko S.A., Lakhtakia A., Yevtushenko O. and Gusakov A.V. 1999 *Phys. Rev.* B **60** 17136

[19] Slepyan G. Ya, Maksimenko S. A., Lakhtakia A., Yevtushenko O. M. and Gusakov A. V. 1998 *Phys. Rev. B* **57** 16 9485

[20] Grigorian L. et al 1999 *Phys. Rev.* B **60** R11309

[21] Sumanasekera G.U., Adu C.K.W., Fang S. and Eklund P.C. 2000 *Phys. Rev. Lett.* **85**, 1096

[22] Mensah S.Y., Allotey F.K.A., Mensah N.G. and Nkrumah G. 2001 *J. Phys. Condens. Matter* **13** 5653

[23] S. Y. Mensah and G. K. Kangah, *J. Phys.: Condens. Matter,* **4** 919 (1992).

[24] Mahan G.D. 1998, Solid State Physics **51** 81.

[25] Rowe D.M., Min G. and Kuznestsov V.L. 1998, *Philosophical Magazine Letters* **77** 105

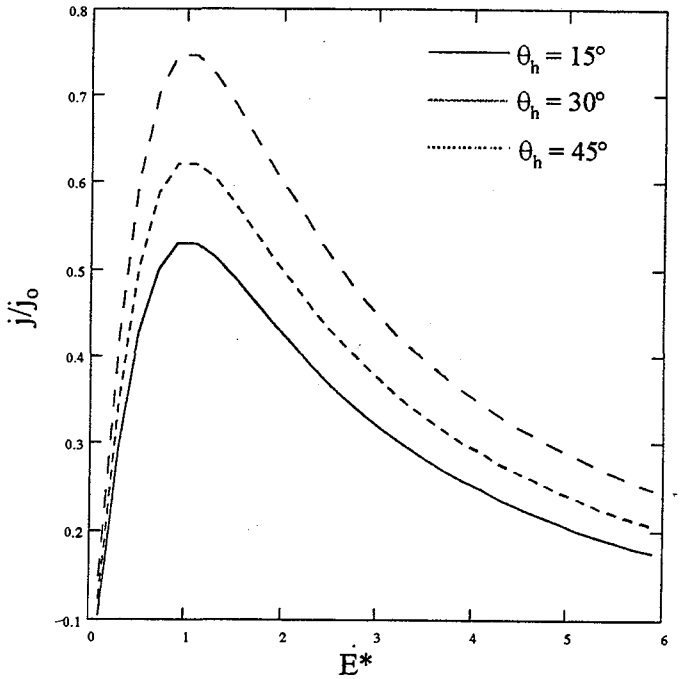

Fig.(1a) Dependence of the normalized current density j/j_o on $E^*(E^* = ed\tau E/\hbar)$ for $\theta_h = 15°$, $30°$ and $45°$.

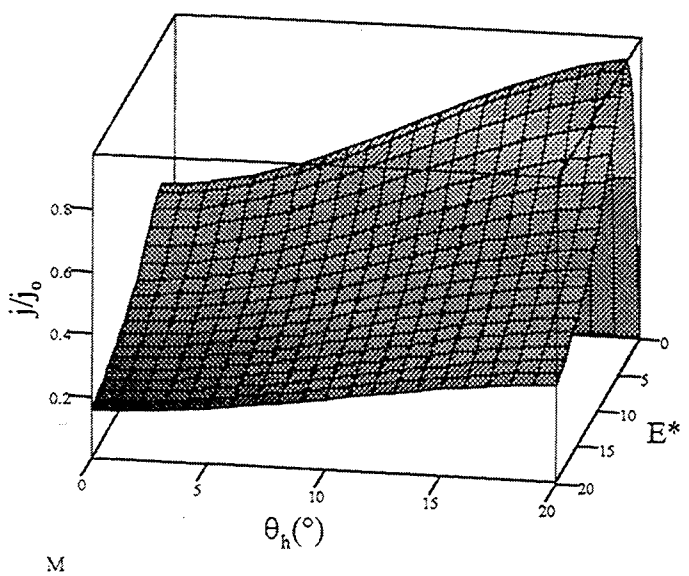

Fig.(1b) Three-demensional plot of the normalized current density j/j_o against E^*. The scale on the E^* axis is 1 unit : 0.299 and that on θ_h axis is 1 unit : 0.068°

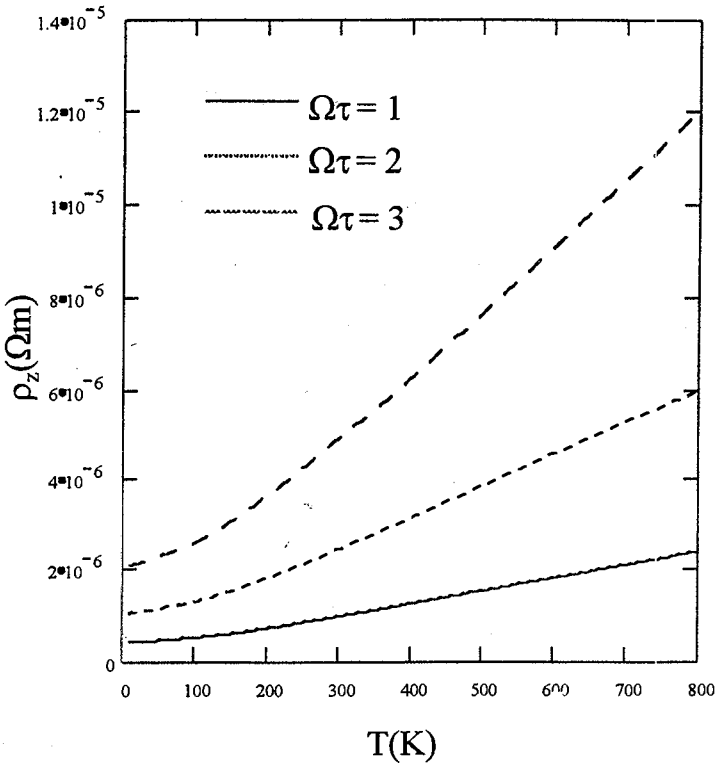

Fig.(2a) Dependence of ρ on T for $\Delta_z = 0.024$eV, $\Delta_s = 0.018$eV and $\theta_h = 8°$.

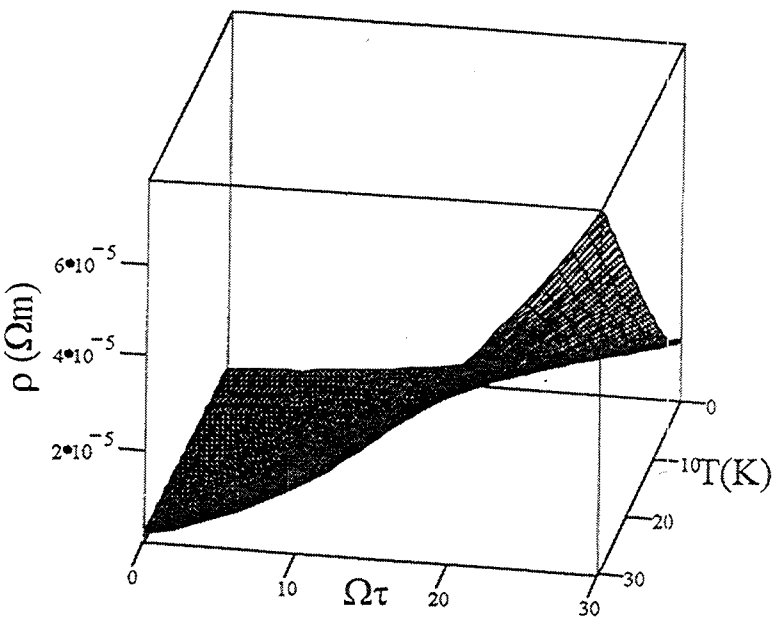

ρ

Fig.(2b) Three-demensional plot of ρ against T and $\Omega\tau$.

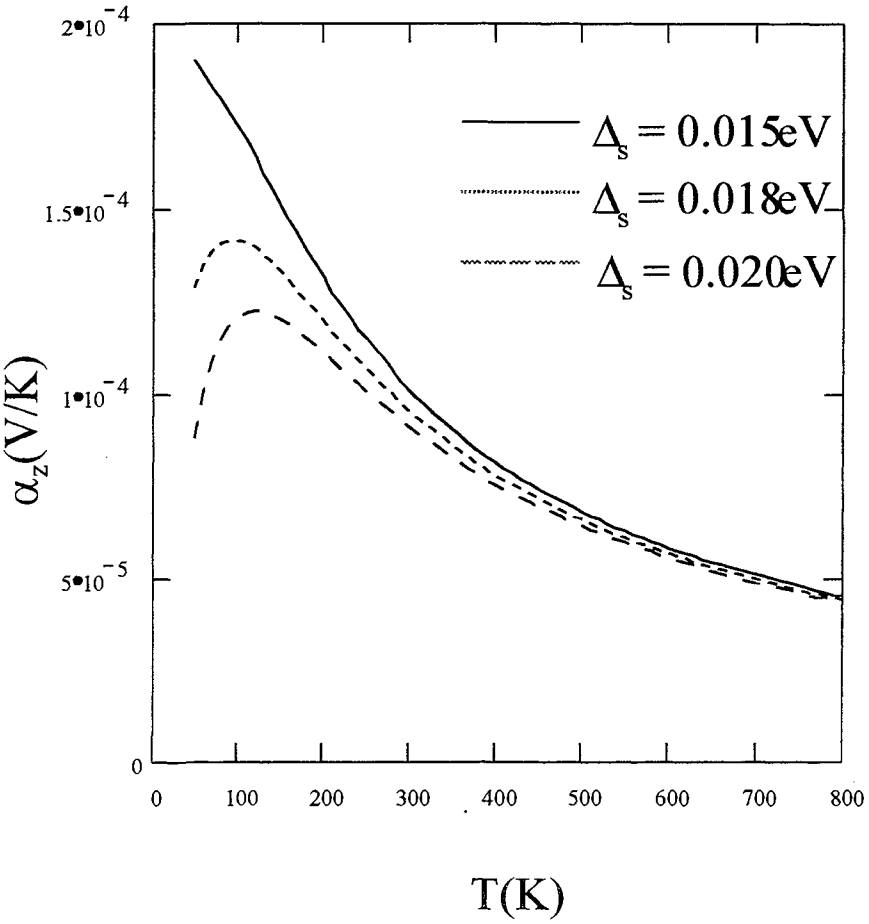

Fig.(3a) A plot of thermopower α_z against temperature T for $\Delta_s = 0.015$eV, 0.018eV and 0.020eV. $\Delta_z = 0.024$eV; $\theta_h = 8°$

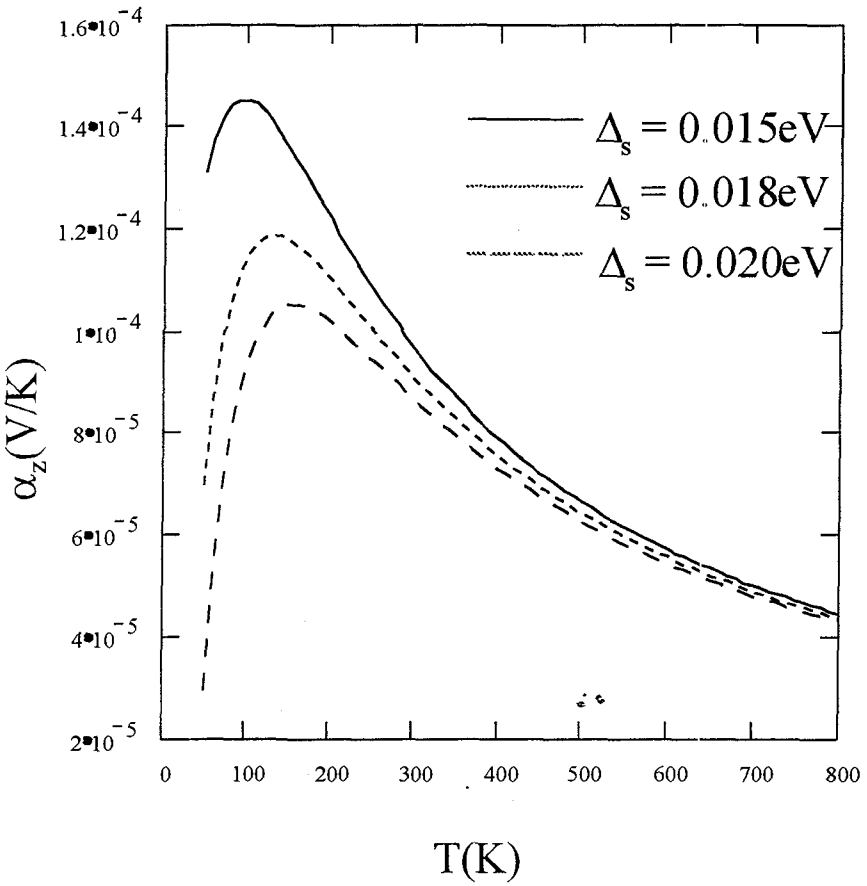

Fig.(3b) A plot of thermpower α_z against temperature T for $\Delta_s = 0.015$eV, 0.018eV and 0.020eV. $\Delta_z = 0.027$eV; $\theta_h = 8°$

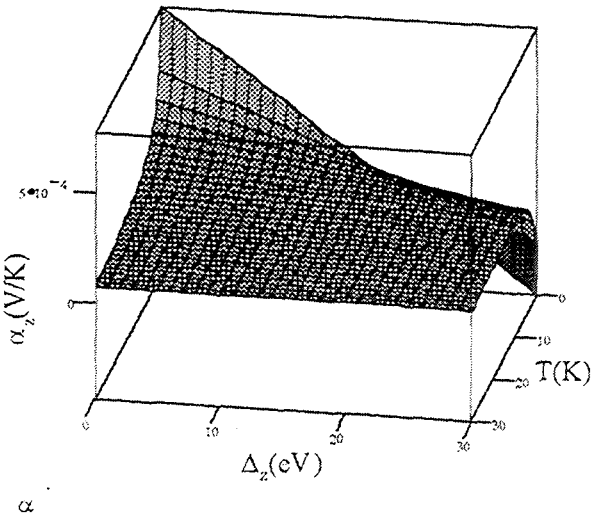

Fig.(3c) A three-dimensional plot of the thermopower α_z against temperature T and Δ_z. $\Delta_s = 0.018$eV; $\theta_h = 8°$ and $\Omega\tau = 1$. The scale on the T axis is 1 unit : 26K and that on the Δ_z axis is 1 unit : 1.3×10^{-3}eV.

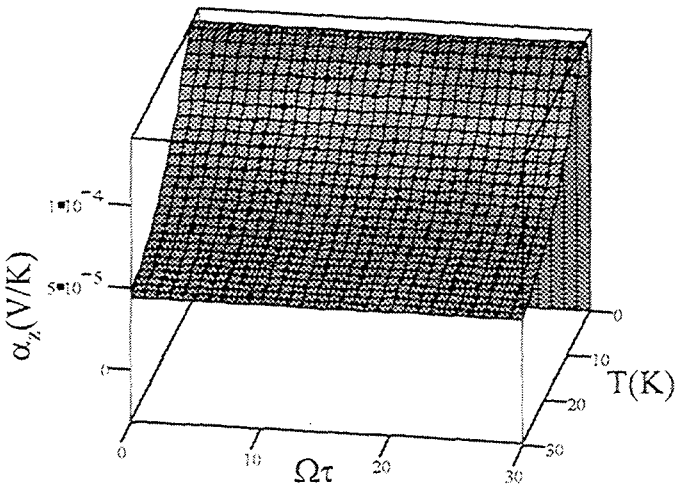

Fig.(3d) A three-demensional plot of α_z against T and $\Omega\tau$. $\Delta_z = 0.024$eV; $\Delta_s = 0.018$eV; and $\theta_h = 8°$. Scale on the T axis is 1 unit : 26.3K and that on the $\Omega\tau$ axis is 1 unit : 0.23

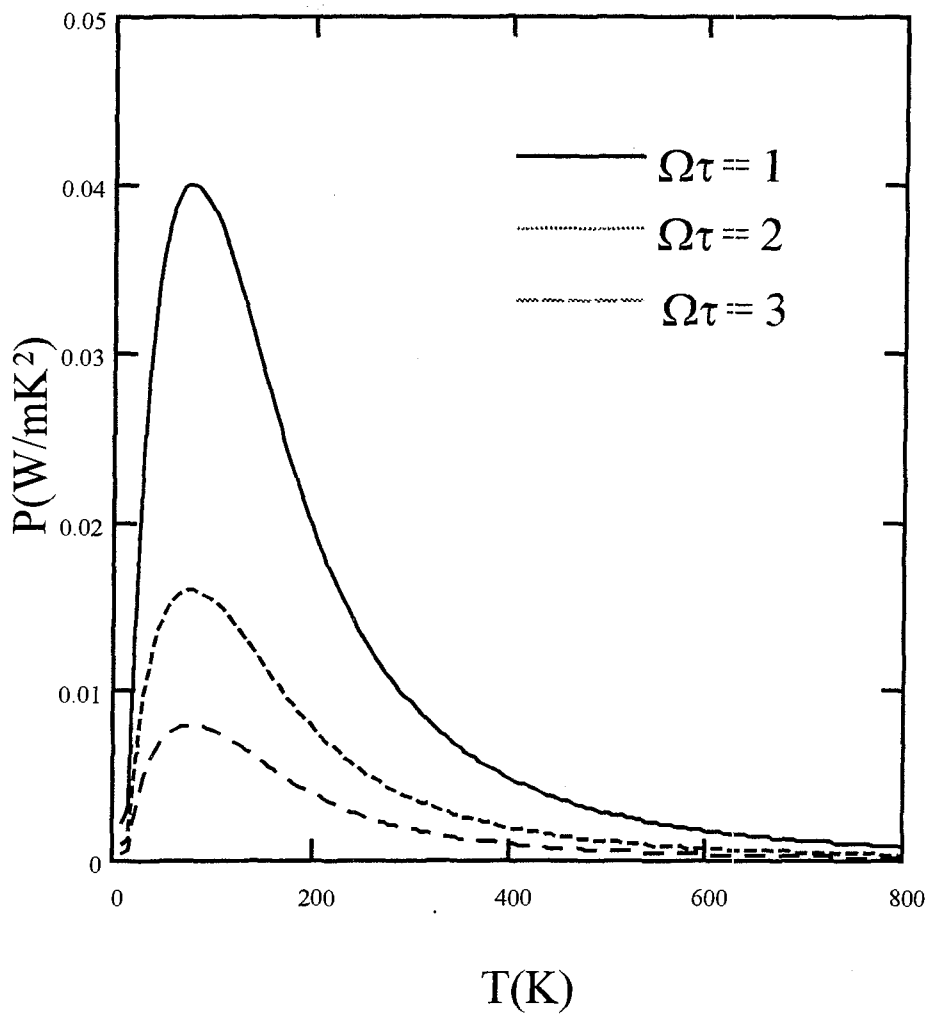

Fig.(4a) Dependence of P on T for $\Omega\tau = 1$, 2 and 3. $\Delta_z = 0.024$eV; $\Delta_s = 0.018$eV and $\theta_h = 8°$

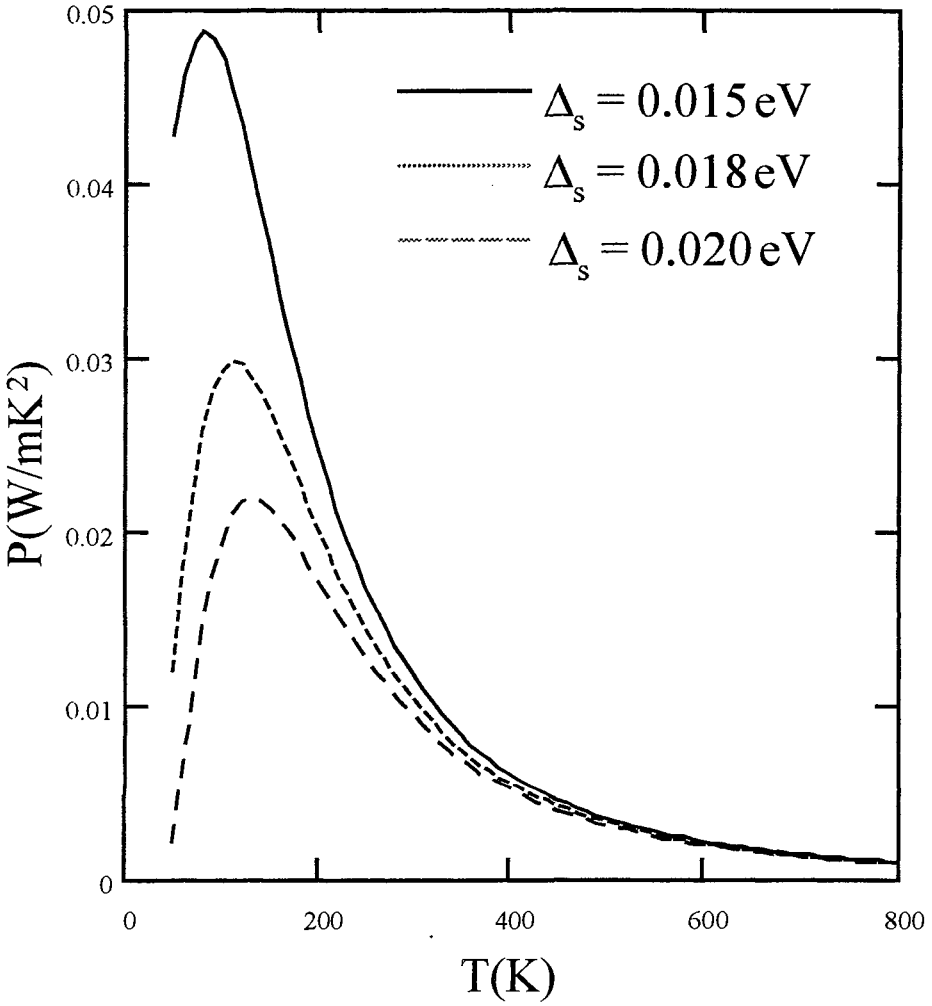

Fig.(4b) A plot of electrical power factor P against temperature T for $\Omega\tau = 1$, 2 and 3. $\Delta_z = 0.027$eV; $\Delta_s = 0.018$eV and $\theta_h = 8°$

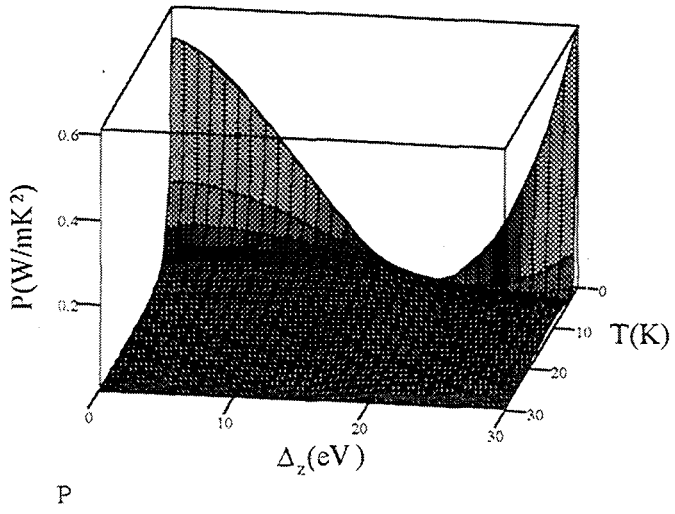

Fig.(4c) A three-demensional plot of P against T and Δ_z. $\Delta_s = 0.018$eV; $\theta_h = 8°$; and $\Omega\tau = 1$. The scale on the T axis is 1 unit : 26K and that on the Δ_z axis is 1 unit : 1.3×10^{-3}eV.

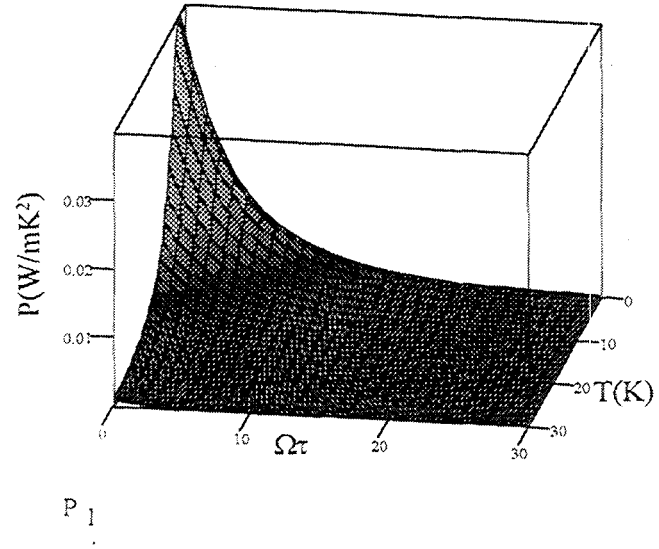

Fig.(4d) A three-dimensional plot of P against T and $\Omega\tau$. $\Delta_z = 0.024$eV; $\Delta_s = 0.018$eV; and $\theta_h = 8°$. Scale on the T axis is 1 unit : 26.3K and that on the $\Omega\tau$ axis is 1 unit : 0.23